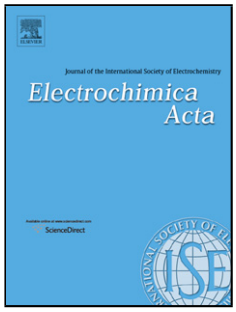

Title: A comparative photophysical and photoelectrochemical study of undoped and 2-aminothiophene-3-carbonitrile-doped carbon nitride

Author: Ana Korina Díaz-García María Isabel Díez-García Teresa Lana-Villarreal Roberto Gómez

PII: S0013-4686(16)32108-9
DOI: http://dx.doi.org/doi:10.1016/j.electacta.2016.10.021
Reference: EA 28109

To appear in: *Electrochimica Acta*

Received date: 13-5-2016
Revised date: 10-9-2016
Accepted date: 4-10-2016

Please cite this article as: Ana Korina Díaz-García, María Isabel Díez-García, Teresa Lana-Villarreal, Roberto Gómez, A comparative photophysical and photoelectrochemical study of undoped and 2-aminothiophene-3-carbonitrile-doped carbon nitride, Electrochimica Acta http://dx.doi.org/10.1016/j.electacta.2016.10.021

A comparative photophysical and photoelectrochemical study of undoped and 2-aminothiophene-3-carbonitrile-doped carbon nitride

Ana Korina Díaz-García, María Isabel Díez-García, Teresa Lana-Villarreal* and Roberto Gómez*

Departament de Química Física i Institut Universitari d'Electroquímica, Universitat d'Alacant, Apartat 99, E-03080 Alicante, Spain

Corresponding authors: roberto.gomez@ua.es; teresa.lana@ua.es

Graphical abstract

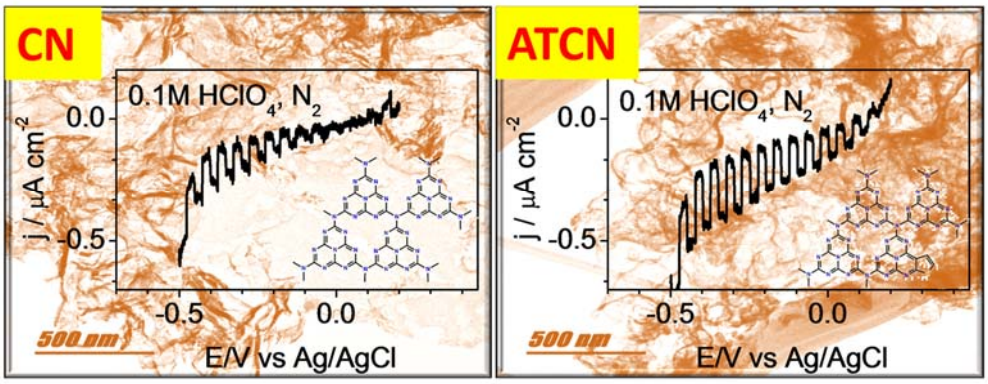

Research highlights

- The effect of molecular doping on carbon nitride is revealed by means of photoelectrochemical and luminescence spectroelectrochemical measurements.
- The effect of pH on the photoelectrochemical response of pristine and doped carbon nitride is presented.

- The intensity of the emission band appearing as a result of molecular doping depends in a reversible way on the applied potential.
- Doped carbon nitride exhibits stronger light absorption and enhanced photocurrents for hydrogen generation.

Abstract

Introducing molecular dopants in carbon nitride has been shown to dramatically modify its electronic structure, resulting in efficient charge separation and improved photocatalytic efficiency. Herein, we have studied the effect of doping carbon nitride with 2-aminothiophene-3-carbonitrile. A fundamental photoelectrochemical characterization has been performed comparing the behavior of the resulting material (ATCN) with carbon nitride (CN). On the one hand, it is shown that the photocurrent onset shifts with the pH up to a value of 8 for both materials, as expected theoretically. On the other, ATCN, which benefits from additional light absorption, shows an improved photoactivity toward hydrogen evolution. In addition, it displays intriguing photoluminescence properties that can be additionally engineered by modulating the potential. In a more general vein, this study illustrates how to shed light on the effects of introducing molecular dopants in the CN matrix.

Keywords: carbon nitride, molecular doping, photoelectrochemistry, hydrogen generation, photoluminescence.

1. Introduction

Global warming and energy crisis are among the main problems that challenge a future viable and sustainable human society. In this context, photocatalytic and photoelectrochemical

devices are promising solutions because of their potential to produce H_2 from H_2O by harvesting solar energy [1-3]. In fact, solar hydrogen would be an excellent alternative fuel since it would be clean, cheap and renewable [4].

Among the different photoactive materials, recently carbon nitride (CN) has attracted much interest for its impressive properties. It stands out due to its thermal and chemical stability, its two-dimensional structure, easy fabrication and semiconductor character, being at the same time a low-cost nontoxic material [5-8]. It is of particular interest that CN features a band gap of about 2.7 eV, with suitable band positions for both water reduction and oxidation [9]. It was first used as a visible light photocatalyst for hydrogen generation by Wang et al. [10]. Since then, a number of publications have appeared demonstrating the interest of this material in photocatalysis [11-17]. However, a low photocatalytic activity has been measured in all cases due to a restricted light absorption and particularly, due to fast charge recombination. The latter has been related with a low surface area, limited charge mobility and the presence of a high density of grain boundary defects [17-19]. However, seeking new strategies to diminish charge recombination or increase light absorption has been a worldwide continuing endeavor and today a number of general approaches have demonstrated to effectively increase the CN limited photoactivity [20]. Namely, doping with metallic or nonmetallic elements, copolymerizing with other organic compounds (see below), performing surface modification (mainly constructing heterojunctions) and nanostructuring are the main successful approaches to increase light absorption and/or favor charge separation.

Carbon nitride is based on covalent networks of tri-s-triazine (heptazine) or triazine units linked by –N= or –NH- groups generating a two dimensional geometry. Being an organic polymer-like material, it can be easily modified through grafting other organic groups in its structure [12,20,22-24]. Among the different possibilities, thiophene-based-π-conjugated molecules have attracted great interest as these motifs can act as strong electron donors and

also as chromophoric centers to harvest photons. On this basis, Wang and coworkers [25-28] have investigated a variety of co-monomers as building blocks to red-shift the optical absorption and promote exciton splitting and charge separation. Among the different co-monomers, 3-aminothiophene-2-carbonitrile has been explored and it has been demonstrated to be particularly promising [25-28]. Its introduction into the CN matrix modulates the electronic structure [25], apparently narrowing the band gap and tuning the LUMO and HOMO positions. This provokes an enhancement in the photocatalytic activity for not only water reduction [25,26,28], but also for the photooxidation of alcohols [27].

Experimentally, this copolymerization takes place simply by heating at 550 ^{o}C the co-monomer with the CN precursor (such as urea, dicyandiamide, etc.). The fact that the co-monomer is introduced in extremely small amounts (about 0.1 %) allows us to consider such a copolymerization as a form of molecular doping. In this regard, doping CN with sulfur has also been studied [29-32]. This element has been introduced using a sulfur atmosphere and also, using organic precursors containing sulfur. Upon doping, an apparent reduction of the band gap is observed as in the case of thiophene-doping. It is expected that sulfur substitutes nitrogen atoms in the CN lattice, changing its electronic structure [33].

In this work, we have prepared carbon nitride via one-pot condensation of urea and sulfur-doped carbon nitride (ATCN) using 2-aminothiophene-3-carbonitrile as a co-monomer. Such a feasible and economic approach leads to chemically improved carbon nitride sheets, as expected. In this contribution, we have tried to shed some light on the main causes that enhance carbon nitride photochemical properties. For such a purpose, we have combined photoelectrochemical and spectroelectrochemical measurements. Our results evince the importance of the disorder degree of the heptazine units in the final behavior, including the possibility of reversibly tuning the luminescence of ATCN samples. The latter fact points to the

presence of new electronic states in ATCN that can act as electron traps. These results disclose new challenges and opportunities for the future development of CN-based materials.

2. Experimental

Nanoporous carbon nitride electrodes were prepared on commercial fluorine-doped tin oxide (FTO) glass substrates (Pilkingon, TEC15) by spin-coating. Carbon nitride powder was obtained by treating 10 g of urea (purity 99.5%+, Aldrich Chem. Co.) in a closed crucible at 550 °C for 2 h (heating ramp of 4 $^{o}C \cdot min^{-1}$). On the other hand, doped carbon nitride powder (ATCN) was obtained by stirring 10 g of urea and 10 mg of 2-aminothiophene-3-carbonitrile (purity 99.99%+, Aldrich Chem. Co.) in 10mL of ultrapure water for 12 hours. Subsequently, the suspension was heated to 80 °C until complete solvent evaporation and treated thermally as described above for the undoped carbon nitride.

Suspensions of the corresponding powders were prepared (5 mg/mL in dimethyl formaldehyde) and spin-coated on FTO using a two-step program: 900 rpm for 9 s and 2000 rpm for 60 s. Afterward, the samples were annealed at 150 °C in air for 10 minutes. The deposition procedure was repeated twice to obtain the desired film thickness (1.8 µm as measured with a mechanical profilometer KLA-Tencor Alpha Step D-100). Finally, the electrodes were post-annealed at 150 °C in air for 40 minutes to partially sinter the particles among them and with the substrate.

A Bruker D8-Advance X-ray diffractometer operating with Cu-Kα radiation at 40 kV and 40 mA was used to obtain the X-ray diffraction patterns. The composition of the electrodes was analyzed by X-ray photoelectron spectroscopy (XPS) using a Kα Thermoscientific spectrometer. The nanoparticle morphology was studied by means of a JEOL JEM-1400 transmission electron

microscope (TEM), while the electrode surface morphology was observed with a JEOL JSM-840 scanning electron microscope (SEM).

Photoelectrochemical measurements were performed at room temperature using a three-electrode cell provided with a fused silica window and a computer-controlled Autolab PGSTAT30 potentiostat. In all cases, an Ag/AgCl/KCl(sat) electrode and a Pt wire were employed as a reference and as a counter electrode, respectively. The linear sweep voltammograms started from the positive potential limit, being the scan performed toward more negative potentials. Five different working electrolytes were used: 0.1 M NaOH, buffer solutions of pH 10.50, 8.0 and 4.7 (Table S1), 0.1 M Na_2SO_4, and 0.1 M $HClO_4$. All of them were prepared with ultrapure water and N_2-purged before the experiments unless otherwise mentioned. The illumination was carried from the electrode substrate side employing a 300 W Xe arc lamp (Thermo Oriel) equipped with a water filter. The light intensity was adjusted with a neutral density filter to 50 $mW \cdot cm^{-2}$ as measured with an optical power meter (Thorlabs model PM100D).

UV-Visible diffuse reflectance spectra were measured with a UV-2401 PC Shimadzu spectrometer using an integrating sphere. Photoluminescence (PL) spectra were recorded using a Fluoromax-4 fluorometer. In-situ luminescence spectroelectrochemical measurements were performed by using an electrochemical cell fitted to a conventional fused silica cuvette. As in the case of the photoelectrochemical measurements, all the potentials were measured against an Ag/AgCl/KCl(sat) reference electrode and a Pt wire was used as a counter electrode. A computer-controlled Autolab PGSTAT30 potentiostat was also used for these experiments.

3. Results

To verify the structure of the as-prepared powders they were analyzed by XRD. The diffractograms of both CN and ATCN are very similar, as displayed in Figure 1. The XRD patterns show two characteristic peaks at about 13 ^{o} and 27.5 ^{o} associated with graphitic stacked CN layers [1,34]. The peak at 13 ^{o} can be indexed as the (100) plane corresponding to the in-plane structural packing motif of tri-s-triazine units, while the intense peak at 27.5 ^{o} corresponds to the graphite-like interlayer (002) plane. It is worth noting that the XRD peaks are broad and relatively weak, indicating low crystallinity due to the presence of small ordered domains and/or a small nanoparticle size.

The sample morphology was characterized by electron microscopy. Representative SEM images of the corresponding electrodes, which are shown in Figures 2A and 2B, indicate that both CN and ATCN samples are composed of porous aggregates. To obtain additional information about the building blocks of such aggregates, CN and ATCN were analyzed by TEM as shown in Figures 2C and 2D. In both cases, a lamellar two-dimensional structure composed of wrinkled nanosheets is observed. From a morphological point of view, both samples are virtually identical.

XPS experiments were carried out to obtain additional information about the chemical composition of both samples (Figure 3). The survey spectrum reveals the presence of three main peaks corresponding to C 1s, N 1s and O 1s. The oxygen peak can be ascribed to the presence of adsorbed impurities such as H_2O or CO_2. The XPS spectra of CN and ATCN show no obvious binding energy shifts for C 1s and N 1s, suggesting that the oxidation state of both elements is basically identical in both samples. The high resolution spectra of N 1s can be separated into three main bands centered at 399.1, 401.0 and 404.9 eV. The peak at 399.1 eV is the most intense and it can be mainly assigned to sp^2 hybridized nitrogen atoms bonded to carbon atoms forming C-N=C units [12,35-36]. This peak could also contain some contribution

of tertiary-nitrogen atoms [34,36]. The peak at 401.0 eV can be related to the presence of some amino functional groups carrying hydrogen $(C)_2$-N-H present in structural defects [12,34,36], but also to tertiary- nitrogen atoms [35]. The peak at 404.9 eV has been ascribed to π excitations [37]. On the other hand, in the high resolution spectra of C 1s, two main contributions at 285.3 and 288.5 eV can be observed. The first can be assigned to sp^3 C-C bonds, coming mainly from carbon-containing contamination, while the latter has been ascribed to carbon atoms coordinated with nitrogen atoms in N-C=N units [12,35,37]. These results indicate the successful generation of a carbon nitride structure based on covalent networks of heptazine units independently of the presence of 2-aminothiophene-3-carbonitrile in the synthesis. Interestingly, in the case of ATCN the presence of sulfur heteroatoms in the final structure coming from thiophene units is also detected in the XPS spectrum. The peak intensity is very low, as expected considering the amount of 2-aminothiophene-3-carbonitrile employed. A sulfur content of 0.04 at % in the final carbon nitride structure can be calculated. The signal from S 2p can be deconvoluted into two contributions centered at 164.6 eV and 165.7 eV. The contribution at 164.6 eV has been ascribed to sulfur atoms substituting nitrogen atoms and forming C-S bonds [31]. The weakest contribution at 165.7 eV has been related to sulfur atoms replacing carbon atoms and generating N-S bonds in the carbon nitride structure [14]. On the basis of these results, we can confirm the incorporation of thiophene units in the CN structure as has been previously proposed for ATCN prepared using 2-aminothiophene-3-carbonitrile and dicyandiamide as precursors (See Fig. S1) [25].

Although the sulfur content is extremely low, it has a profound effect on the light absorption spectra of the samples. The color changes from pale yellow (for CN powder) to light brown upon doping in agreement with previous results and theoretical calculations for both thiophene-doped [25-28] but also sulfur-doped carbon nitride [33,38]. Figure 4 shows the diffuse UV-visible reflectance spectra in Kubelka-Munk units. As observed, the light absorption

is larger for ATCN than for CN in the full spectrum range. In addition, the absorption edge is red shifted in the case of ATCN from about 460 nm (2.7 eV) to 600 nm (2.1 eV) due to the appearance of a feature at around 500 nm. Based on density functional theory (DFT) calculations of single layers of carbon nitride [39], Jorge et al. analyzed the UV-vis diffuse reflectance and the photoluminescence spectra of CN prepared at different temperatures [19]. These authors observed that, as the synthesis temperature increases, the CN absorption edge shifts to longer wavelengths and an additional feature emerges near 500 nm so that the samples become yellow-brown similarly to the case of thiophene/sulfur-doping. These authors assigned the intense band in the UV region to π–π* transitions. The feature that appears near 500 nm with increasing reaction temperature was interpreted as due to n–π* transitions, involving lone pair electrons of the N atoms at the edge of the heptazine units. Moreover, the authors assumed that such n–π* transitions are forbidden for perfectly symmetric and planar heptazine units and they become allowed when the heptazine units developed some distortions [39]. This assignment was confirmed by Yu et al. [40], who also considered the possible influence of CN-interlayer electron coupling. Analogously, in the case of ATCN, it is expected that the presence of thiophene groups and/or sulfur atoms in the final structure can induce the distortion of conjugated heptazine units and therefore, the existence of an absorption band at around 500 nm. Such an improved light absorption of the modified samples has been related to their improved photocatalytic behavior [26].

Remarkably, CN has been previously employed to carry out both photoinduced oxidation and reduction reactions [5,8,23,41]. To rationalize such a particular behavior, photoelectrochemical measurements were performed in different media for CN and ATCN. Figure 5A shows linear sweep voltammograms under transient illumination for CN and ATCN electrodes in O_2-purged 0.1 M $HClO_4$. Depending on the applied potential a cathodic or an anodic photocurrent appears. A similar behavior has been reported for polyheptazine electrodes using an acetonitrile-based electrolyte [42]. No alteration of the

photoelectrochemical response was detected during the experiments, which suggests the absence of fast degradation processes. The cathodic photocurrents and dark currents are assigned to oxygen reduction. The observed ambivalent behavior can be understood on the basis of the nanostructured character of the electrodes combined with an unlikely separation of the photogenerated electron-hole pairs. Under such conditions, the charge collection is dominated by the kinetics of the different carrier transfer and transport processes, being the driving force for charge transport modulated by controlling the substrate potential. Thus, the transport of either electrons or holes can be favored in nanoporous electrodes, changing the photocurrent sign. In fact, even in the case of classical n-type electrodes such as TiO_2 electrodes, they can behave as photocathodes depending on the electrolyte composition and applied potential [43]. Interestingly, the photoelectrochemical behavior is similar for CN and ATCN electrodes although the current in the dark is significantly larger for ATCN, which indicates that this material is a better electrocatalyst for oxygen reduction than undoped CN. In addition, a saturation of the dark cathodic current is apparent in the case of the ATCN electrode. This is probably linked to the facts that the doping level is low and that the thiophene moieties may act as catalytic centers for oxygen reduction.

In the absence of oxygen (Figure 5B), the cathodic photocurrents for both CN and ATCN electrodes are significantly smaller than in its presence and start at more negative potentials. This is due to the fact that oxygen is a better electron acceptor than water/protons, thus recombination is favored in its absence. Interestingly, ATCN electrodes develop photocurrents significantly larger than CN, that is, they are more photoactive for hydrogen generation. This improvement in the photoelectrochemical behavior could be related with different factors. The introduction of thiophene units in the CN structure could: (a) increase the number of electron-hole pairs generated (as a larger portion of the UV-Visible spectrum can be harvested), (b) improve the photogenerated charge separation, (c) modify the charge transport (due to doping and/or structural changes in the heptazine units arrangement (see

below)), (d) vary the electrocatalytic properties of the surface (modifying the electron transfer rate). It is worth noting the fact that, in the presence of oxygen, the photocurrent is only slightly larger for ATCN samples, while in its absence it is significantly larger. This is a good indication that the main factor making CN photocathode less effective than ATCN is not related with charge transport. If this were the case, transport would equally limit the photoelectrochemical behavior of CN in the presence of oxygen. In any case, the photocurrents are very low. In fact, even when sophisticated procedures are employed for improving the photoelectrochemical response of CN electrodes, only modest photocurrents are achieved [44,45].

We have studied the photocurrent onset potential for CN and ATCN electrodes in different electrolytes (Fig. S2). Such a potential, measured in the presence of a good electron scavenger, is of key importance as it gives an estimate of the flat band potential which should be close to the valence band edge location in the case of ideal p-type electrodes. However, CN and ATCN electrodes are far from being ideal, as evidenced by their ambivalent behavior. This lack of ideality is also illustrated by reports showing positive-slope Mott-Schottky plots, indicative of an n-type character, even when cathodic photocurrents are detected [46]. Thus, the onset potential can be considered only as a pseudo flat band potential. In any case, it is a critical parameter for evaluating the suitability of a photoelectrode for water splitting tandem devices. This potential cannot be theoretically calculated as it depends not only on the material itself, but also on the charge state of its surface. In aqueous media in the absence of strong adsorbed species, the pH and the material isoelectric point (IEP) determine whether the semiconductor surface is positively or negatively charged. This is particularly the case of oxide semiconductors such as TiO_2, where the surface metal atoms act as Lewis acid sites adsorbing hydroxide anions, while the surface bridging oxygen atoms attract protons, acting as Lewis base sites. In these cases, as the pH increases, the band edges at the semiconductor surface shift upward (in the energy scale), that is, downward in the electrode potential scale. The expected shift at 298

K is of ~ 0.059 V/pH unit. In the case of carbon nitride, water adsorption has been theoretically studied [46-48]. However, to the best of our knowledge, no thorough study of the IEP for CN materials and the possible influence of the presence of different functional groups or dopants has been published. The shift of the conduction and valence band edges with pH also remains an open question.

Figure 6A shows the values of the photocurrent onset potential as a function of pH for CN and ATCN electrodes immersed in electrolytes of different pH in the presence of oxygen. The onset potential becomes more negative as the pH increases and exhibits a linear behavior between pH 1 and 8. In this range, a Nernstian behavior is roughly observed with a slope close to 59 mV per pH unit. This behavior agrees with the fact that carbon nitride can be reversibly protonated in contact with mineral acids, thus modifying its solubility/dispersability and surface area [50]. However, for values of pH higher than 8, the onset potential remains almost constant. This presumably means that all the functional groups present in carbon nitride are fully deprotonated already at pH 8. No meaningful differences in the onset potential have been detected for CN and ATCN in the presence of oxygen. This can be due to the fact that the presence of thiophene/sulfur moieties does not significantly alter the surface charge state and that the pseudo-flat band potential are virtually the same for both materials. Obviously, the surface charge state could be altered due to the presence of new functional groups in ATCN, which could hidden the expected shift of the pseudo-flat band potential upon doping.

In the absence of oxygen, recombination is favored and the onset of the photocurrent shifts toward more negative values as can be observed in Figure 6B. In this regard, the ATCN samples exhibit values for the onset potential slightly more positive than CN, which is indicative of a more efficient electron-hole pair separation in the doped samples, in agreement with the larger observed photocurrent.

In order to obtain additional information about the recombination processes of the photogenerated charge carriers, PL measurements were carried out. Generally speaking, the faster the separation of the electron-hole pairs, the higher the photoactivity and the lower the PL. Figure 7 shows the steady-state PL spectra corresponding to CN and ATCN electrodes, excited with 380 nm light. The emission spectra correspond well with the absorption spectra. An intense band with a maximum at around 440 nm is observed for CN. The spectrum clearly differs from that of ATCN: this PL peak is red-shifted to 460 nm and an additional broad band appears centered at 510 nm for ATCN.

Most authors have related the carbon nitride PL to that observed for hydrogenated carbons with different levels of nitrogen content [50,51]. Accordingly, the origin of the PL activity at around 400 nm is supposed to be the recombination of electron-hole pairs in atomic domains with sp^2 hybridization, involving π^*-π transitions. The fact that the peak shifts from 440 nm to 460 nm for the ATCN sample indicates a stronger orbital overlap, probably because the π conjugated system is enhanced due to the presence of thiophene/sulfur moieties. On the other hand, the feature at 510 nm has also been observed for CN samples treated at high temperatures [19,52,53] and for samples treated with hydrogen [54,55]. In these cases, this peak has been related with the emission associated with π^*-n transitions, which, as mentioned above, is allowed for distorted samples (for instance, buckled CN layers), heptazine units without planar symmetry, or triazine units without a trigonal symmetry. Hence, this result points to a larger defect concentration in ATCN. Furthermore, the emission is larger for ATCN than for CN, indicating a larger radiative recombination for ATCN, which is in apparent contrast with its higher photoelectrochemical activity.

To obtain further information about recombination/trapping of photogenerated charge carriers, PL measurements were carried out in situ in the course of electrochemical experiments. An ATCN electrode in N_2-purged 0.1 M Na_2SO_4 (pH~6) was excited with 380 nm

light, while the potential was stepped, and both the current and the emitted light were measured simultaneously. As observed, in Figure 8 the intensity of the emitted light at 525 nm can be modulated by switching the applied potential. Light emission increases in the potential range where cathodic photocurrents are developed (Figure 8A) while it diminishes at positive potentials (Figure 8B). As revealed by repeating the potentiostatic steps, this phenomenon is fully reversible. In contrast, emission at 450 nm for CN electrodes is barely affected by applied potential. Note that the currents shown in Figure 8, are due to dark processes occurring after switching the potential. The magnitude of the photocurrent due to the incident light coming from the fluorometer should be extremely small due to its low intensity.

Several works have been published about cathodic electroluminescence using carbon nitride electrodes [56,57]. In these cases, the luminescence was detected in the presence of oxygen or other electron acceptor species and it was related to the ability of CN to inject hot electrons and generate radicals in aqueous media. In our case, this possibility can be discarded because: (a) the PL intensity remains constant for an undoped CN electrode (see Figure 8C and 8D) and (b) the PL intensity can be also modulated at potentials where no cathodic currents are detected (Figure 8B). Therefore, we can clearly ascribe the PL to the photophysics of the charge carriers. Accordingly, this result implies that the π*-n transitions, which are allowed for ATCN electrodes, are enhanced as the applied potential becomes more negative. Similar experiments performed with ATCN electrodes but recording the PL at 450 nm also showed an increase in the PL signal at negative potentials (Fig. S3), although the enhancement was slightly smaller. The additional promotion of π*-n transitions in the potential range where the photocurrent is enhanced, allows us to propose that the degree of distortion of the heptazine units increases in this potential range, being such a change in the organization reversible.

4. Discussion

ATCN was prepared using the same procedure as for CN but introducing a small amount of 2-aminothiophene-3-carbonitrile in the precursor mixture. This has allowed us to prepare samples with basically the same morphology at a microscopic level and characterized by a layered structure. The photoelectrochemical characterization has shown that both materials are photoactive for hydrogen evolution. At sufficiently negative potentials, cathodic photocurrents are generated, being larger for ATCN electrodes. Although these currents are still too modest for practical applications, the low cost of the active materials combined with their environmentally friendly character and the possibility of harvesting visible light make these electrodes still attractive. Such a low photoactivity can be linked to a fast electron-hole recombination due to a restricted charge carrier mobility and to a high exciton binding energy [17,18,19,58].

Doping CN with thiophene motifs induces important changes in the material electronic structure as evinced by both absorption and emission spectra. These spectra are red-shifted for ATCN and, in addition, they show a new feature at longer wavelengths in agreement with previous experimental results [25-28]. Reported DFT calculations also reveal important modifications in the electronic structure upon grafting a thiophene group in a heptazine trimer [25]: the π electrons are relocalized and thus the HOMO (i.e. the valence band edge) and the LUMO (i.e. the conduction band edge) levels are affected. In pristine CN, the HOMO level is homogeneously distributed throughout the CN plane, while in the case of the doped sample it is mainly located in the heptazine containing the thiophene unit. In contrast, the LUMO level remains basically unaffected upon the introduction of the thiophene unit and spans uniformly through the CN plane. The rather different spatial location of the HOMO and the LUMO in the ATCN sample is thought to facilitate the separation of photoinduced electron hole pairs. In addition, the DFT calculations also show that there is an important up-shift of the HOMO level and a minor down-shift of the LUMO level, resulting in a smaller band gap and thus in a red-shifted spectrum.

On the other hand, the absorption/fluorescence at about 450 nm has been ascribed mainly to π*-π transitions, while the new feature appearing at longer wavelengths in the ATCN has been ascribed to π*-n transitions, which are possible only for distorted carbon nitride structures. This implies that the presence of thiophene/sulfur in ATCN induces structural defects that can be linked to the presence of additional wrinkles in the nanosheets, to a collapse of the planar symmetry of some heptazine units, or to the loss of the trigonal symmetry of some triazine units.

Coupling PL and electrochemical measurements evinces that applying a negative potential induces an enhancement of the PL mainly in the case of ATCN, particularly at wavelengths corresponding to π*-n transitions. Interestingly, the PL enhancement kinetics seems to be correlated with the developed cathodic currents (Fig. S4). Such currents appearing upon shifting the potential toward more negative values can be ascribed mainly to charge accumulation, as only capacitive currents are detected in this potential range (Fig. S5).

Putting together all the pieces of information and, in contrast to the expected behavior, we can conclude that at negative potentials both photoactivity (i.e. charge separation) and luminescence (i.e. radiative charge recombination) are promoted. We can tentatively explain the observed behavior by considering that, at negative potentials, nanoporous semiconductor electrodes can accumulate electrons by filling electronic states in the band gap. Such accumulation could deactivate possible non-radiative recombination channels competing with emission.

Generally speaking, non-equilibrium electrons recombine with holes in the valence band by undergoing either a band-to-band transition or a transition that involves some acceptor levels or traps. The different processes expected to occur in ATCN electrodes have been summarized in Figure 9. As detailed previously, depending on the energy of the incident photons, excitation occurs in ATCN π→π* (1) or n→π* (3) followed by a rapid radiative electron hole

recombination (through transitions 2 and 4). Our experimental data, point to the existence of electron traps that could capture π* conduction band electrons (5). This process is expected to be very fast. Subsequently, trapped electrons recombine with n and π valence band holes non-radiatively (6) via a Shockley-Read-Hall like mechanism. This second step is expected to be slower as it involves hole diffusion and also the trapping cross section may be small. When a negative potential is applied, electrons are accumulated in the nanoporous electrode filling these traps. Once the traps are filled, they are saturated and cannot capture further electrons; thus the non-radiative recombination path becomes deactivated. As a result radiative electron-hole recombination is promoted. Trap-filling has been shown to enhance the PL quantum yield in a number of very different semiconducting samples such as quantum dots [60], TiO_2 nanotubes [61] and perovskite thin films [62]. The fact that, only in the case of ATCN, PL is modulated by applied potential clearly indicates that the electron traps are associated to the presence of thiophene/sulfur moieties.

On the other hand, the accumulation of electrons in a nanoporous ATCN electrode has to be accompanied by the adsorption/insertion of protons to preserve electroneutrality. In fact carbon nitride has been proposed as a material for hydrogen storage and also for lithium ion batteries [59,60]. This process could provoke changes in the material structure due to expansion. Such a structural change would lead to a more defective and disordered CN framework. This could explain the additional promotion of the n-π* transitions and the slow kinetics of the PL decay upon shifting the potential toward positive values.

Finally and as expected, the photoactivity is larger for ATCN than for CN electrodes [25-28]. The larger cathodic photocurrent exhibited by ATCN can be related to the more distorted arrangement of the graphitic planes. Such a matrix distortion allows harvesting a larger portion of the UV-visible spectrum. Hence, as the samples are illuminated with the full spectrum of a Xe(Hg) arc lamp, a larger number of electron-hole pairs can be generated. In addition, some

authors have pointed out that these defects would improve charge separation and transfer (catalytic sites) [65]. In fact, a high exciton binding energy leading to a low dissociation probability at room temperature has been reported for carbon nitride [59]. We believe that the as-generated defects in ATCN are vital for charge separation; however the role of the thiophene/sulfur moieties as electron donor dopants should not be disregarded. A higher electron concentration could favor electron transport to the particle surface, where the reaction takes place. The idea of an improved charge separation for ATCN agrees well with both the shift observed for the photocurrent onset potential and the photocurrent values in the absence of an electron scavenger. Finally, considering the extremely small amount of thiophene/sulfur incorporated in the ATCN matrix, it seems that the effect of doping and disorder are not simply additive, but probably synergetic.

5. Conclusions

We have prepared carbon nitride via condensation of urea and carbon nitride doped with 2-aminothiophene-3-carbonitrile. The fundamental electrochemical characterization of both materials shows that the photocurrent onset potential becomes more negative with the pH for both nitrogen and oxygen purged electrolytes and exhibits an approximately Nernstian behavior between pH 1 and 8. Experimental results also show that both CN and ATCN can develop cathodic photocurrents ascribed to hydrogen evolution, being larger for ATCN. However, the photocurrents measured are still very low for practical applications.

To gain further insights into the behavior of CN and ATCN, we have tried to relate their photoelectrochemical properties to their structures and optoelectronic properties. In contrast to CN, the π^*-n transitions are allowed for ATCN as revealed by the absorption and emission spectra in the visible region. These transitions have been related to a structural distortion of the planar heptazine units, which allows ATCN to harvest more efficiently visible photons.

Combining electrochemical and spectroscopic measurements, we have shown that PL in ATCN can additionally be modulated in a reversible way by modulating the potential. Such a behavior has been related to the presence of electronic traps in ATCN and to the fact that the structure of ATCN depends on applied potential in a reversible way.

The high impact caused by the introduction of thiophene/sulfur moieties in the CN structure indicates that useful future research may be focused on CN and other photoactive materials with well-controlled structural defects as they may tune the electronic structure and could introduce active sites.

Acknowledgments

We are grateful to the Spanish Ministry of Education and Competitiveness for financial support through projects MAT2012-37676 and MAT2015-71727-R (co-financed with FEDER funds by the European Union). A.-K.D.G. thanks the Mexican government (CONACYT) for the award of a doctoral grant.

Apendix A. Supplementary data

Supplementary data associate with this article can be found, in the online version.

References

[1] S.Z. Wu, Y.X. Yu, W. De Zhang, Processing graphitic carbon nitride for improved photocatalytic activity, Mater. Sci. Semicond. Process. 24 (2014) 15–20.

[2] Y. Tian, B. Chang, Z. Yang, B. Zhou, F. Xi, X. Dong, Graphitic carbon nitride–$BiVO_4$

heterojunctions: simple hydrothermal synthesis and high photocatalytic performances, RSC Adv. 4 (2014) 4187–4193.

[3] F. Yang, V. Kuznietsov, M. Lublow, C. Merschjann, A. Steigert, J. Klaer, A. Thomas, T. Schedel-Niedrig, Solar hydrogen evolution using metal-free photocatalytic polymeric carbon nitride/CuInS2 composites as photocathodes, J. Mater. Chem. A. (2013) 6407–6415.

[4] M. Schröder, K. Kailasam, S. Rudi, M. Richter, a. Thomas, R. Schomäcker, M. Schwarze, Impact of the reaction conditions on the photocatalytic reduction of water on mesoporous polymeric carbon nitride under sunlight irradiation, Int. J. Hydrogen Energy. 39 (2014) 10108–10120.

[5] J. Zhu, P. Xiao, H. Li, S. a C. Carabineiro, Graphitic carbon nitride: synthesis, properties, and applications in catalysis., ACS Appl. Mater. Interfaces. 6 (2014) 16449–65.

[6] G. Dong, Y. Zhang, Q. Pan, J. Qiu, A fantastic graphitic carbon nitride (g-C3N4) material: Electronic structure, photocatalytic and photoelectronic properties, J. Photochem. Photobiol. C Photochem. Rev. 20 (2014) 33–50.

[7] S. Cao, J. Yu, g-C3N4-Based Photocatalysts for Hydrogen Generation, J. Phys. Chem. Lett. 5 (2014) 2101–2107.

[8] X. Wang, S. Blechert, M. Antonietti, Polymeric graphitic carbon nitride for heterogeneous photocatalysis, ACS Catal. 2 (2012) 1596–1606.

[9] Z. Xing, Z. Chen, X. Zong, L. Wang, A new type of carbon nitride-based polymer composite for enhanced photocatalytic hydrogen production, Chem. Commun. 50 (2014) 6762-6764.

[10] X. Wang, K. Maeda, A. Thomas, K. Takanabe, G. Xin, J.M. Carlsson, K. Domen, M.

Antonietti, A metal-free polymeric photocatalyst for hydrogen production from water under visible light, Nat. Mater. 8 (2009) 76–80.

[11] X. Fan, L. Zhang, M. Wang, W. Huang, Y. Zhou, M. Li, R. Cheng, J. Shi, Constructing carbon-nitride-based copolymers via Schiff base chemistry for visible-light photocatalytic hydrogen evolution, Appl. Catal. B Environ. 182 (2016) 68–73.

[12] J. Qin, S. Wang, H. Ren, Y. Hou, X. Wang, Photocatalytic reduction of CO2 by graphitic carbon nitride polymers derived from urea and barbituric acid, Appl. Catal. B Environ. 179 (2015) 1–8.

[13] N. Wang, Y. Zhou, C. Chen, L. Cheng, H. Ding, A g-C3N4 supported graphene oxide/Ag3PO4 composite with remarkably enhanced photocatalytic activity under visible light, Catal. Commun. 73 (2016) 74–79.

[14] K. Wang, Q. Li, B. Liu, B. Cheng, W. Ho, J. Yu, Sulfur-doped g-C3N4 with enhanced photocatalytic CO2-reduction performance, Appl. Catal. B Environ. 176–177 (2015) 44–52.

[15] J. Jiang, J. Yu, S. Cao, Au/PtO nanoparticle-modified g-C3N4 for plasmon-enhanced photocatalytic hydrogen evolution under visible light, J. Colloid Interface Sci. 461 (2016) 56–63.

[16] X.D. Sun, Y.Y. Li, J. Zhou, C. Hai Ma, Y. Wang, J.H. Zhu, Facile synthesis of high photocatalytic active porous g-C3N4 with ZnCl2 template, J. Colloid Interface Sci. 451 (2015) 108–116.

[17] J. Lin, Z. Pan, X. Wang, Photochemical Reduction of CO 2 by Graphitic Carbon Nitride Polymers, ACS Sustain. Chem. Eng. 2 (2014) 353–358.

[18] Y. Zhang, Z. Schnepp, J. Cao, S. Ouyang, Y. Li, J. Ye, S. Liu, Biopolymer-Activated

Graphitic Carbon Nitride towards a Sustainable Photocathode Material, Sci. Rep. 3 (2013) 1–5.

[19] a. B. Jorge, D.J. Martin, M.T.S. Dhanoa, A.S. Rahman, N. Makwana, J. Tang, A. Sella, F. Corà, S. Firth, J. a. Darr, P.F. McMillan, H2 and O2 evolution from water half-splitting reactions by graphitic carbon nitride materials, J. Phys. Chem. C. 117 (2013) 7178–7185.

[20] Y. Zheng, L. Lin, B. Wang, X. Wang, Graphitic Carbon Nitride Polymers toward Sustainable Photoredox Catalysis, Angew. Chemie Int. Ed. (2015) 12868–12884.

[21] J. Gao, J. Wang, X. Qian, Y. Dong, H. Xu, R. Song, C. Yan, H. Zhu, Q. Zhong, G. Qian, J. Yao, Journal of Solid State Chemistry One-pot synthesis of copper-doped graphitic carbon nitride nanosheet by heating Cu – melamine supramolecular network and its enhanced visible-light-driven photocatalysis, J. Solid State Chem. 228 (2015) 60–64.

[22] J. Zhang, X. Chen , K. Takanabe, K. Maeda, K. Domen, J.D. Epping, X. Fu, M. Antonietti, X. Wang , Synthesis of a Carbon Nitride Structure for Visible-Light Catalysis by Copolymerization, Angew. Chemie Int. Ed. 49 (2010) 441–444.

[23] J. Zhang, G. Zhang, X. Chen, S. Lin, L. Möhlmann, G. Dołęga, G. Lipner, M. Antonietti, S. Blechert, X. Wang, Co-monomer control of carbon nitride semiconductors to optimize hydrogen evolution with visible light, Angew. Chemie - Int. Ed. 51 (2012) 3183–3187.

[24] T. Jordan, N. Fechler, J. Xu, T.J.K. Brenner, M. Antonietti, M. Shalom, “caffeine Doping” of Carbon/Nitrogen-Based Organic Catalysts: Caffeine as a Supramolecular Edge Modifier for the Synthesis of Photoactive Carbon Nitride Tubes, ChemCatChem. 7 (2015) 2826–2830.

[25] J. Zhang, M. Zhang, S. Lin, X. Fu, X. Wang, Molecular doping of carbon nitride photocatalysts with tunable bandgap and enhanced activity, J. Catal. 310 (2014) 24–30.

[26] M. Zhang, X. Wang, Two dimensional conjugated polymers with enhanced optical absorption and charge separation for photocatalytic hydrogen evolution, Energy Environ. Sci. 7 (2014) 1902-1906.

[27] Y. Chen, J. Zhang, M. Zhang, X. Wang, Molecular and textural engineering of conjugated carbon nitride catalysts for selective oxidation of alcohols with visible light, Chem. Sci. 4 (2013) 3244-3248.

[28] D. Zheng, C. Pang, Y. Liu, X. Wang, Shell-engineering of hollow g-C_3N_4 nanospheres via copolymerization for photocatalytic hydrogen evolution, Chem. Commun. 51 (2015) 9706–9709.

[29] G. Liu, P. Niu, C. Sun, S.C. Smith, Z. Chen, G.Q. Lu, H.M. Cheng, Unique electronic structure induced high photoreactivity of sulfur-doped graphitic C3N4, J. Am. Chem. Soc. 132 (2010) 11642–11648.

[30] J. Hong, X. Xia, Y. Wang, R. Xu, Mesoporous carbon nitride with in situ sulfur doping for enhanced photocatalytic hydrogen evolution from water under visible light, J. Mater. Chem. 22 (2012) 15006-15012.

[31] L.-L. Feng, Y. Zou, C. Li, S. Gao, L.-J. Zhou, Q. Sun, M. Fan, H. Wang, D. Wang, G.-D. Li, X. Zou, Nanoporous sulfur-doped graphitic carbon nitride microrods: A durable catalyst for visible-light-driven H2 evolution, Int. J. Hydrogen Energy. 39 (2014) 15373–15379.

[32] J. Chen, Z. Hong, Y. Chen, B. Lin, B. Gao, One-step synthesis of sulfur-doped and nitrogen-deficient g-C3N4 photocatalyst for enhanced hydrogen evolution under visible light, Mater. Lett. 145 (2015) 129–132.

[33] Y.Z. Xinguo Ma, Yanhui Lv, Jing Xu, Yanfang Liu, Ruiqin Zhang, A Strategy of Enhancina the Photoactivity of g-C3N4 via Doping of Nonmetal Element: A First-Principles Study, J.

Phys. Chem. C. 116 (2012) 23485–23493.

[34] A. Thomas, A. Fischer, F. Goettmann, M. Antonietti, J.-O. Müller, R. Schlögl, J.M. Carlsson, Graphitic carbon nitride materials: variation of structure and morphology and their use as metal-free catalysts, J. Mater. Chem. 18 (2008) 4893-4908.

[35] Y. Chen, B. Wang, S. Lin, Y. Zhang, X. Wang, Activation of n → π* Transitions in Two-Dimensional Conjugated Polymers for Visible Light Photocatalysis, J. Phys. Chem. C. 118 (2014) 29981–29989.

[36] W.-K.H. Fan Dong, Zaiwang Zhao, Ting Xiong, Ziling Ni, Wendong Zhang, Yanjuan Sun, In Situ Construction of g-C3N4/g-C3N4 Metal-Free Heterojunction for Enhanced Visible-Light Photocatalysis, ACS Appl. Mater. Interfaces. 5 (2013) 11392–11401.

[37] J. Liu, T. Zhang, Z. Wang, G. Dawson, W. Chen, Simple pyrolysis of urea into graphitic carbon nitride with recyclable adsorption and photocatalytic activity, J. Mater. Chem. 21 (2011) 14398-14401.

[38] S. Stolbov, S. Zuluaga, Sulfur doping effects on the electronic and geometric structures of graphitic carbon nitride photocatalyst: insights from first principles, J. Phys. Condens. Matter. 25 (2013) 85507.

[39] M. Deifallah, P.F. McMillan, F. Cora, F. Cor\gravea, Electronic and Structural Properties of Two-Dimensional Carbon Nitride Graphenes, J. Phys. Chem. C. 112 (2008) 5447–5453.

[40] H. Zhang, A. Yu, Photophysics and photocatalysis of carbon nitride synthesized at different temperatures, J. Phys. Chem. C. 118 (2014) 11628–11635.

[41] Z. Zhao, Y. Sun, F. Dong, Graphitic carbon nitride based nanocomposites: a review, Nanoscale. 7 (2015) 15–37.

[42] M. Bledowski, L. Wang, A. Ramakrishnan, O. V Khavryuchenko, V.D. Khavryuchenko, P.C. Ricci, J. Strunk, T. Cremer, C. Kolbeck, R. Beranek, Visible-light photocurrent response of TiO2-polyheptazine hybrids: evidence for interfacial charge-transfer absorption., Phys. Chem. Chem. Phys. 13 (2011) 21511–9.

[43] T. Lana-Villarreal, R. Gómez, Tuning the photoelectrochemistry of nanoporous anatase electrodes by modification with gold nanoparticles: Development of cathodic photocurrents, Chem. Phys. Lett. 414 (2005) 489–494.

[44] J. Liu, H. Wang, Z.P. Chen, H. Moehwald, S. Fiechter, R. Van De Krol, L. Wen, L. Jiang, M. Antonietti, Microcontact-printing-assisted access of graphitic carbon nitride films with favorable textures toward photoelectrochemical application, Adv. Mater. 27 (2015) 712–718.

[45] J. Xu, S. Cao, T. Brenner, X. Yang, J. Yu, M. Antonietti, M. Shalom, Supramolecular Chemistry in Molten Sulfur: Preorganization Effects Leading to Marked Enhancement of Carbon Nitride Photoelectrochemistry, Adv. Funct. Mater. 25 (2015) 6265–6271.

[46] J. Zhang, X. Chen, K. Takanabe, K. Maeda, K. Domen, J.D. Epping, X. Fu, M. Antonieta, X. Wang, Synthesis of a carbon nitride structure for visible-light catalysis by copolymerization, Angew. Chemie - Int. Ed. 49 (2010) 441–444.

[47] S.M. Aspera, M. David, H. Kasai, First-Principles Study of the Adsorption of Water on Tri-s -triazine-based Graphitic Carbon Nitride, Jpn. J. Appl. Phys. 49 (2010) 115703.

[48] H.-Z. Wu, L.-M. Liu, S.-J. Zhao, The effect of water on the structural, electronic and photocatalytic properties of graphitic carbon nitride, Phys. Chem. Chem. Phys. 16 (2014) 3299-3304.

[49] H.-Z. Wu, L.-M. Liu, S.-J. Zhao, The role of the defect on the adsorption and dissociation

of water on graphitic carbon nitride, Appl. Surf. Sci. 358 (2015) 363–369.

[50] Y. Zhang, A. Thomas, M. Antonietti, X. Wang, Activation of carbon nitride solids by protonation: Morphology changes, enhanced ionic conductivity, and photoconduction experiments, J. Am. Chem. Soc. 131 (2009) 50–51.

[51] Rusli, J. Robertson, G.A.J. Amaratunga, Photoluminescence behavior of hydrogenated amorphous carbon, J. Appl. Phys. 80 (1996) 2998–3003.

[52] X. Bai, C. Cao, X. Xu, Q. Yu, Synthesis and characterization of crystalline carbon nitride nanowires, Solid State Commun. 150 (2010) 2148–2153.

[53] Y. Kang, Y. Yang, L.-C. Yin, X. Kang, G. Liu, H.-M. Cheng, An Amorphous Carbon Nitride Photocatalyst with Greatly Extended Visible-Light-Responsive Range for Photocatalytic Hydrogen Generation, Adv. Mater. 27 (2015) 4572–4577.

[54] C. Merschjann, T. Tyborski, S. Orthmann, F. Yang, K. Schwarzburg, M. Lublow, M.-C. Lux-Steiner, T. Schedel-Niedrig, Photophysics of polymeric carbon nitride: An optical quasimonomer, Phys. Rev. B. 87 (2013) 205204.

[55] X. Li, G. Hartley, A.J. Ward, P.A. Young, A.F. Masters, T. Maschmeyer, Hydrogenated Defects in Graphitic Carbon Nitride Nanosheets for Improved Photocatalytic Hydrogen Evolution, J. Phys. Chem. C. 119 (2015) 14938–14946.

[56] W. Ho, Z. Zhang, M. Xu, X. Zhang, X. Wang, Y. Huang, Enhanced visible-light-driven photocatalytic removal of NO: Effect on layer distortion on g-C3N4 by H2 heating, Appl. Catal. B Environ. 179 (2015) 106–112.

[57] L. Chen, D. Huang, S. Ren, T. Dong, Y. Chi, G. Chen, Preparation of graphite-like carbon nitride nanoflake film with strong fluorescent and electrochemiluminescent activity, Nanoscale. 5 (2013) 225–230.

[58] Q. Jiang, S. Anna-Maria, H. Markus, S. Johanna, A.-K. Timo, K. Sakari, Electrochimica Acta, Electrochim. Acta. 51 (2006) 2706–2714.

[59] S. Melissen, T. Le Bahers, S.N. Steinmann, P. Sautet, The Relationship Between Carbon Nitride Structure and Exciton Binding Energies: A DFT Perspective, J. Phys. Chem. C. (2015) 25188-25196.

[60] C. Galland, Y. Ghosh, A. Steinbrück, M. Sykora, J. a Hollingsworth, V.I. Klimov, H. Htoon, Two types of luminescence blinking revealed by spectroelectrochemistry of single quantum dots., Nature. 479 (2011) 203–7.

[61] C. Wehrenfennig, C.M. Palumbiny, H.J. Snaith, M.B. Johnston, L. Schmidt-Mende, L.M. Herz, Fast Charge-Carrier Trapping in TiO2 Nanotubes, J. Phys. Chem. C. 119 (2015) 9159–9168.

[62] Y. Tian, M. Peter, E. Unger, M. Abdellah, K. Zheng, T. Pullerits, A. Yartsev, V. Sundström, I.G. Scheblykin, Mechanistic insights into perovskite photoluminescence enhancement: light curing with oxygen can boost yield thousandfold, Phys. Chem. Chem. Phys. 17 (2015) 24978–24987.

[63] M. Wu, Q. Wang, Q. Sun, P. Jena, Functionalized Graphitic Carbon Nitride for Efficient Energy Storage.pdf, J. Phys. Chem. C. 117 (2013) 6055–6059.

[64] T.S. Miller, A.B. Jorge, A. Sella, F. Corà, P.R. Shearing, D.J.L. Brett, P.F. McMillan, The use of graphitic carbon nitride based composite anodes for lithium-ion battery applications, Electroanalysis. (2015) 2614–2619.

[65] H. Wang, X. Zhang, J. Xie, J. Zhang, P. Ma, B. Pan, Y. Xie, Structural distortion in graphitic-C3N4 realizing an efficient photoreactivity., Nanoscale. 7 (2015) 5152–6.

Figure captions

Figure 1. XRD patterns for CN and ATCN powders.

Figure 2. SEM (A,B) and TEM (C,D) images for CN (A,C) and ATCN (B,D) samples (films and powders).

Figure 3. XPS survey spectra (A), and high-resolution XPS spectra of N 1s region (B), C 1s region (C) and S 2p region (D) for CN and ATCN samples.

Figure 4. UV-Visible diffuse reflectance spectra in Kubelka-Munk units for CN and ATCN samples.

Figure 5. Linear scan voltammograms for CN and ATCN electrodes in (A) O_2-purged 0.1 M $HClO_4$ and (B) N_2-purged 0.1 M $HClO_4$ under transient illumination with an ozone-free Xe arc lamp. Scan rate: 5 $mV \cdot s^{-1}$. Scan direction: negative-going.

Figure 6. Onset potential of the photocurrent as a function of pH in the presence (A) and in the absence (B) of O_2 for both CN and ATCN electrodes in contact with a 0.1M $HClO_4$ solution. Illumination source: ozone-free Xe arc Lamp.

Figure 7. Steady-state PL spectra for CN and ATCN under 380 nm excitation.

Figure 8. Simultaneous chronoamperometric and luminescence measurements for ATCN (A and B) and CN (C and D) electrodes in N_2-purged 0.1 M Na_2SO_4 using 380 nm light for photoexcitation. The potential is stepped from -250 mV to -750 mV (A and C) and from -250 mV to 500 mV (B and D).

Figure 9. Schematic representation of the processes responsible for light absorption and PL in ATCN samples. Solid arrows show processes involving photons and dashed arrows show non-radiative processes. Incident photons generate electron-hole pairs due to $\pi \rightarrow \pi^*$ (1) or $n \rightarrow \pi^*$ (3) transitions depending on the incident wavelength. These carriers can recombine either via band to band transitions emitting a photon (2 and 4) or through unoccupied acceptor states (6). The latter is expected to be a non-radiative process. However, if such acceptor levels or traps are already filled, trapping (5) cannot occur and thus recombination via (6) cannot procced, leading to an enhancement of the radiative recombination processes (2 and 4).

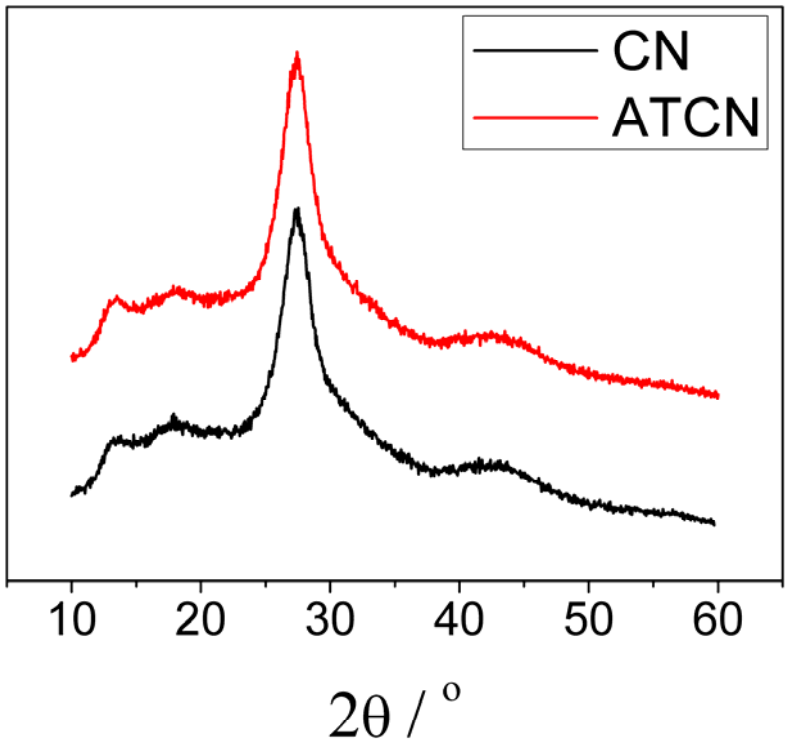

Fig 1

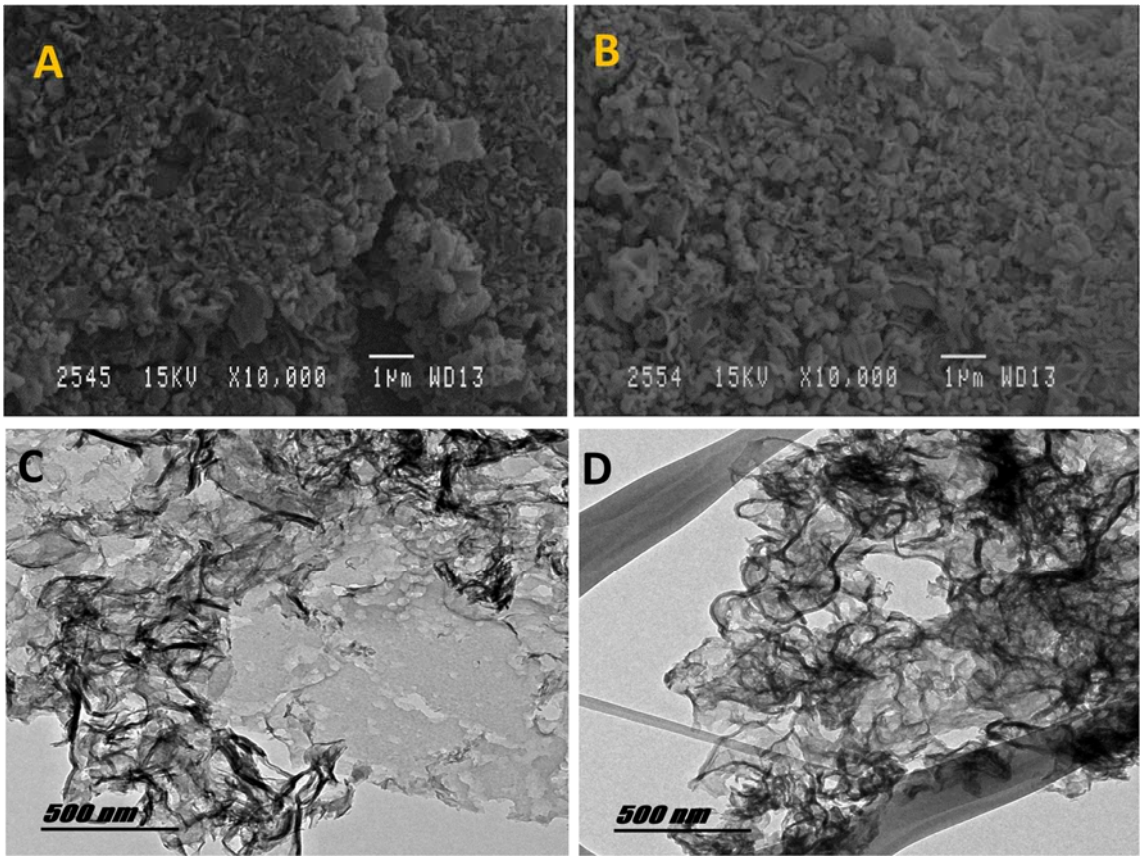

Fig2

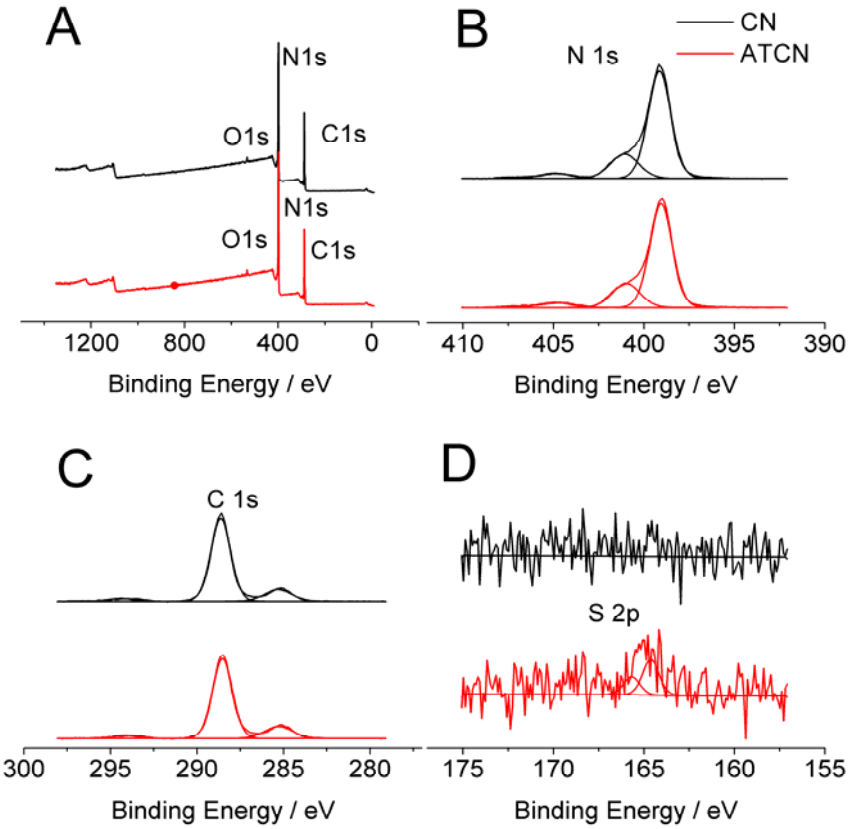

Fig 3

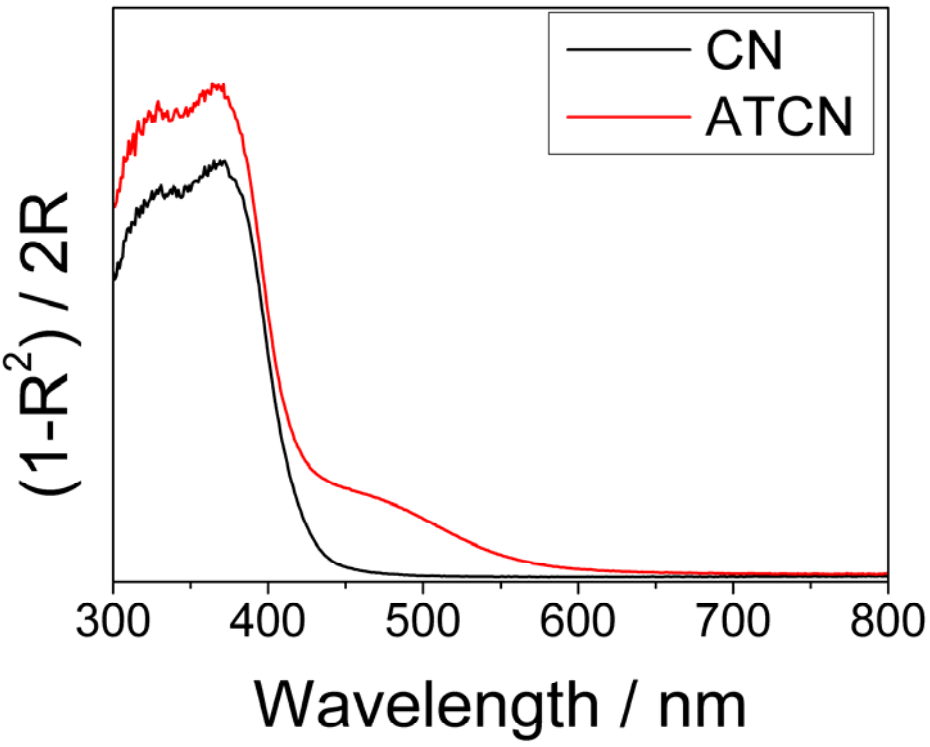

Fig 4

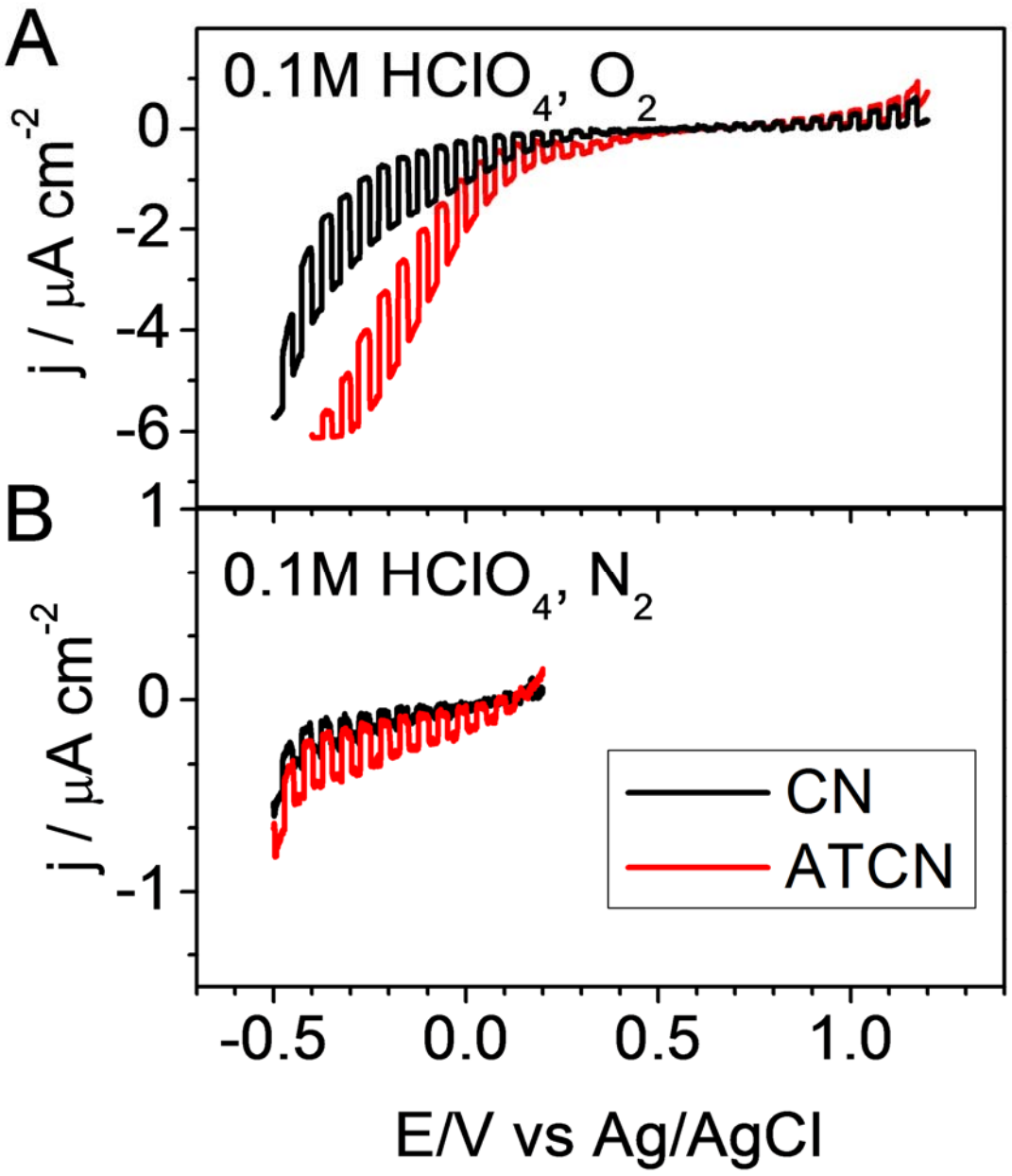

Fig 5

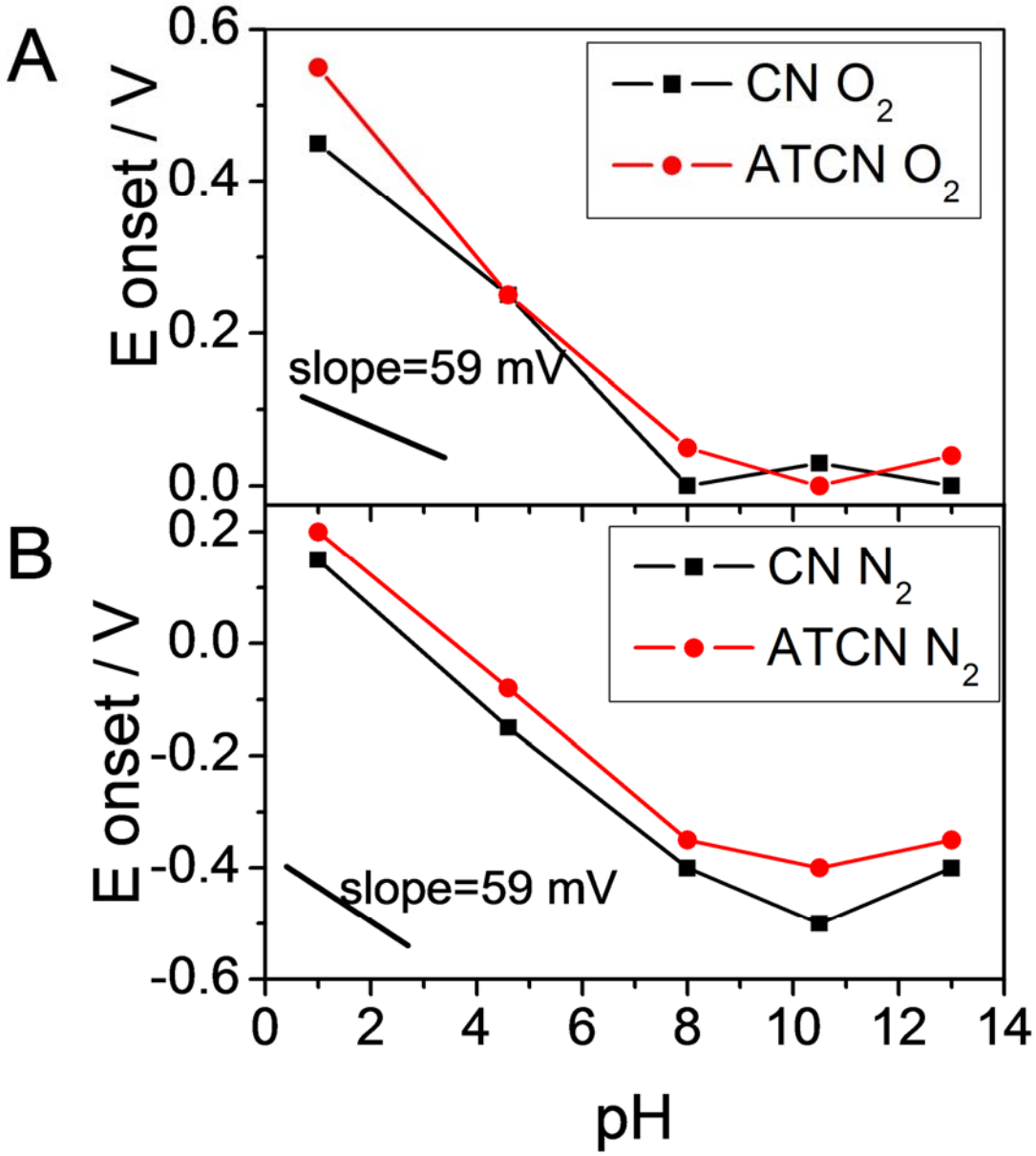

Fig 6

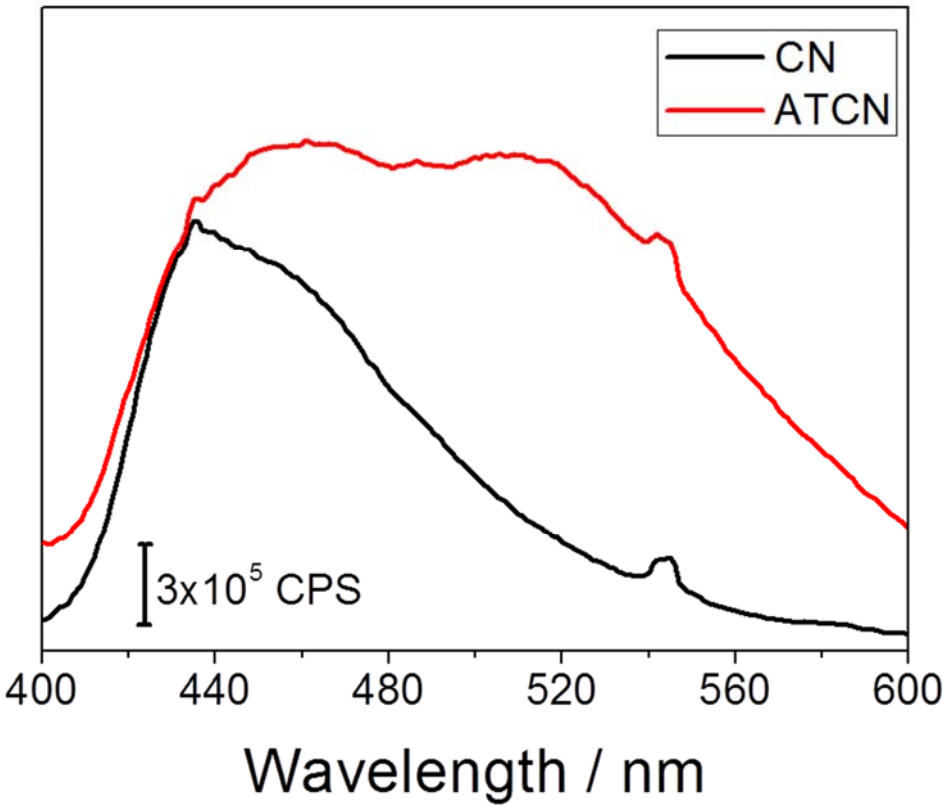

Fig 7

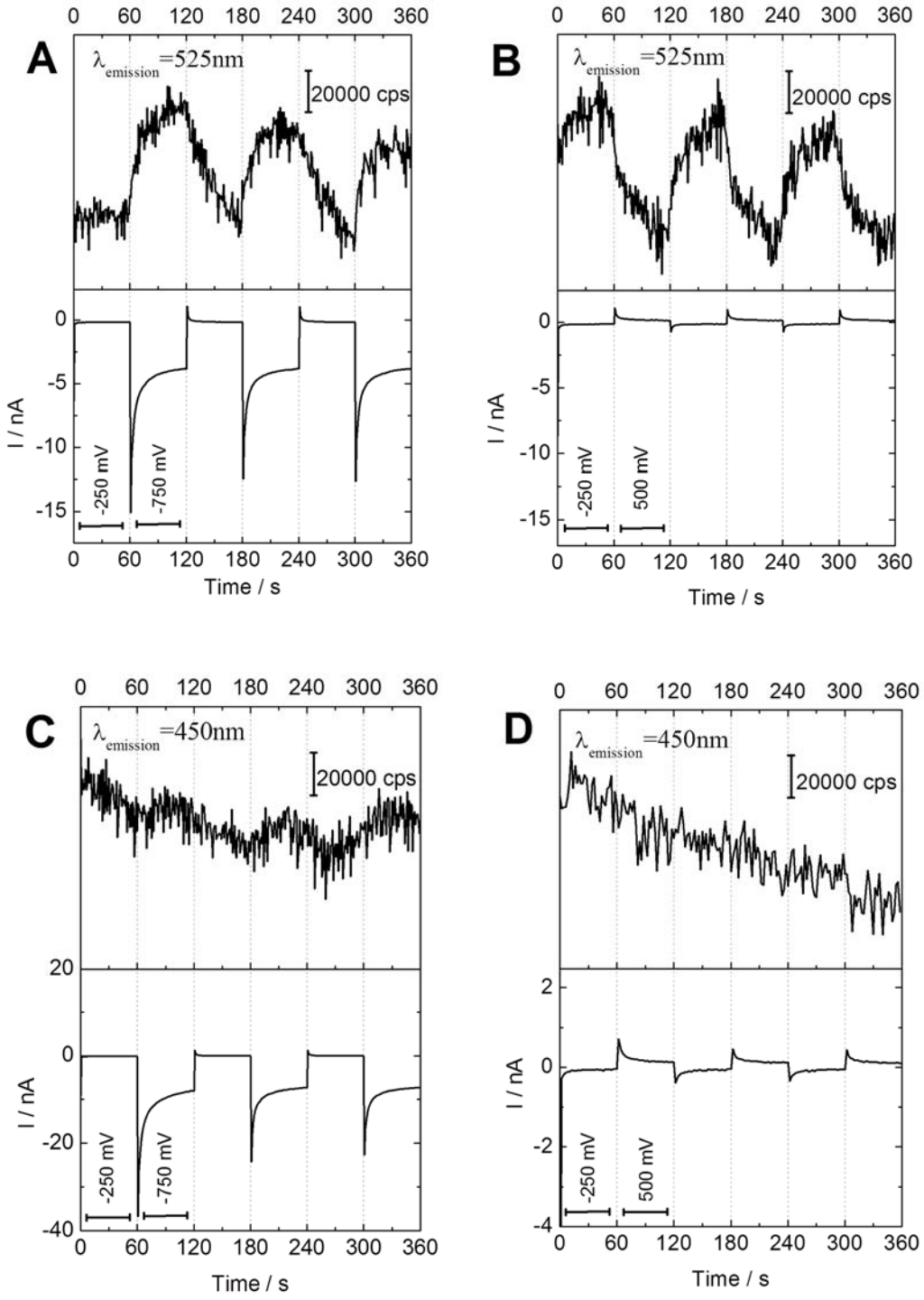

Fig 8

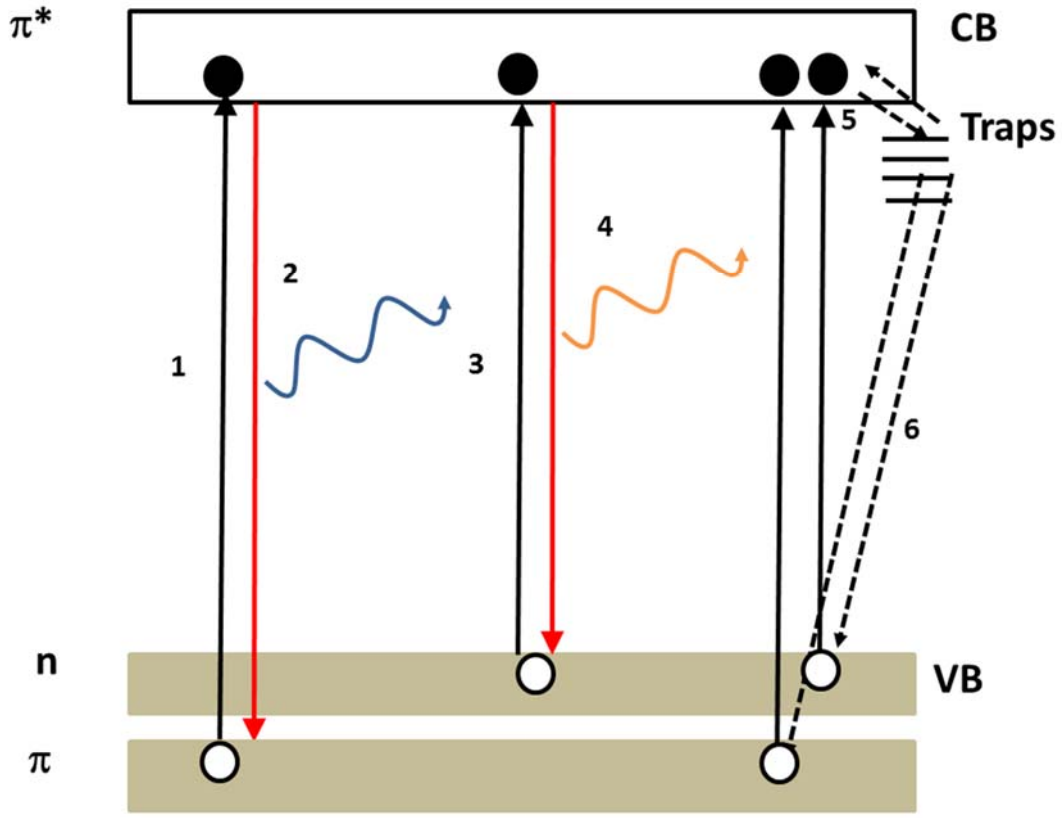

Fig 9